RSC Advances

PAPER

View Article Online
View Journal | View Issue

Cite this: *RSC Adv.*, 2025, **15**, 1507

Application of MMP-2-responsive *in situ* forming injectable hydrogel in preventing the recurrence of oral squamous cell carcinoma

Wei Li, †[a] Yan Wang,†[b] Hongkun Miao,†[c] Maohui Yan,[d] Chen Liu,[d] Yu Wang,*[c] Jianjun Zhang *[a] and Zhiguang Fu*[d]

Received 23rd August 2024
Accepted 3rd December 2024

DOI: 10.1039/d4ra06120a

rsc.li/rsc-advances

Oral squamous cell carcinoma is one of the most common types of cancer. Surgical resection is one of the most important treatments at present. However, patients often suffer from regional recurrence after surgery. Therefore, new strategies for combination therapy need to be investigated. This work identified a smart injectable hydrogel system co-delivering DOX and sunitinib nanoparticles. The nano drugs are continuously released from the hydrogels and effectively taken up by cells. The nano drugs in the hydrogel can inhibit tumor cell viability and induce cancer cell apoptosis *in vitro*. The drug-loaded hydrogel could control the recurrence of subcutaneous xenograft tumors, prolong the survival time, and have no obvious toxicity in nude mice. These findings suggest that this smart injectable hydrogel system may provide new ideas for the comprehensive treatment of oral squamous cell carcinoma.

Introduction

Oral squamous cell carcinoma (OSCC) is the most common malignant epithelial tumor in the oral, maxillofacial, and head and neck regions, accounting for approximately 90% of cases.[1] The prevention and treatment of OSCC is a difficult task. In the past 30 years, although the treatment concepts and methods have been continuously updated,[2–4] the treatment effect has been unsatisfactory. As far as OSCC is concerned, surgery is still the main treatment, and the thoroughness of radical surgery is the key to ensuring the survival of patients after surgery.[5,6] However, due to the complex anatomical structure of the oral and maxillofacial region, as well as the lack of unified criteria for the evaluation of the existing surgical safety margins and other factors, the recurrence and treatment failure of the tumor after surgery eventually led to an increase in patient mortality.[7–9] Therefore, controlling postoperative recurrence has been one of the critical problems in the clinical treatment of OSCC.

In most solid tumors, cancer cells stimulate the formation of new blood vessels by secreting various growth factors, such as vascular endothelial growth factor (VEGF), to meet the demand for oxygen and nutrients of the tumor.[10] The newly formed blood vessels in tumors are often defective, exhibiting characteristics such as disorganized proliferation, impaired vascular function, and a hypoxic microenvironment.[11] The disordered structure of blood vessels within tumors hampers the delivery of anti-cancer drugs to deeper tumor regions, reducing the effectiveness of these therapies.[12] Antiangiogenic therapy, such as sunitinib, competes with the kinase sites of vascular endothelial growth factor receptor (VEGFR) to bind to VEGF and prevent its binding to its receptor, thereby inhibiting angiogenesis to promote normalization of the tumor blood vessels and improve vascular permeability and distribution.[13] Normal blood vessels can increase the concentration of anti-cancer drugs within the tumor. Therefore, combining anti-angiogenesis drugs with anti-cancer drugs may enhance the effectiveness of tumor treatment.

Hydrogels as drug carriers have been effectively applied in tumor recurrence prevention.[14,15] Utilizing the high expression of MMP-2 in the tumor microenvironment, enzyme-responsive hydrogels are developed for cancer therapy.[16–18] Drug-loaded enzyme-responsive hydrogels in tumor sites enable the responsive release of drugs.[19] Most anticancer drugs are hydrophobic and face challenges in dispersing within hydrogels. Reducing the size of hydrophobic drugs to the nanoscale can help to alleviate this problem.[20]

In this study, an MMP-2-responsive, *in situ* forming hydrogel co-delivering anticancer drugs is employed to address post-operative recurrence of OSCC (Scheme 1). Angiogenesis plays a crucial role in the tumor recurrence process. Sunitinib is a multi-targeted receptor tyrosine kinase inhibitor that inhibits angiogenesis and the proliferation of tumor cells.[21] Doxorubicin is a broad-spectrum anticancer drug.[22] Both drugs are

[a]*College of Chemical Engineering, Beijing University of Chemical Technology, Beijing, 100029, China. E-mail: zhangjj@mail.buct.edu.cn*

[b]*Department of Internal Neurology, 309 Hospital of PLA, Beijing 100091, China*

[c]*Department of Oncology, Air Force Medical Center, PLA, Beijing, 100142, China. E-mail: wangyufmmu@163.com*

[d]*Department of Radiotherapy, Air Force Medical Center, The Fourth Military Medical University, PLA, No. 30 Fucheng Road, Haidian District, Beijing 100142, China. E-mail: xiaochuan8668@126.com*

† W. Li, Y. Wang, and H. Miao contributed equally to this work.

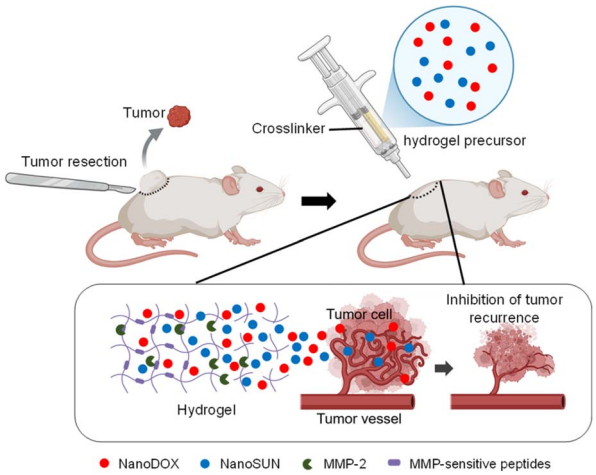

Scheme 1 Schematic representation showing the mechanism of the drug-loaded hydrogel on tumor therapy. After the subcutaneous tumor in the mice was resected, the drug-loaded hydrogel was implanted into the tumor site. Within the tumor microenvironment, MMP-2 degrades the MMP-sensitive peptides in the hydrogel structure, and drugs are gradually released from the hydrogel to inhibit angiogenesis and tumor recurrence.

formulated as nanoparticles using an amphiphilic block copolymer and are encapsulated within the hydrogel. This drug delivery system shows promising applications in treating postoperative recurrence of OSCC.

Materials and methods

Materials

Doxorubicin hydrochloride (DOX·HCl) was brought from the Zhongshuo Pharmaceutical Technology Development Co., Ltd, Beijing, China. Sunitinib (SUN), polyethylene glycol (PEG, M_n = 10 kDa), adipic dihydrazide (ADH), and 1-ethyl-3-[3-dimethylaminopropyl] carbodiimide hydrochloride EDC were purchased from Aladdin. D,L-Lactide (D,L-LA) was purchased from the Daigang Biomaterial Co., Ltd, Jinan, China. Tin 2-ethylhexanoate was purchased from Sigma. Sodium hyaluronan (HA, M_n = 60 kDa) was purchased from the Bloomage Freda Biopharm Co., Ltd, Jinan, China. *N*-Acryloxysuccinimde (NAS) was purchased from J&K Scientific Ltd, Beijing, China. MMP-sensitive peptides (GCRDGPQGIWGQDRCG) were synthesized by Scilight Biotechnology (Beijing, China). Active matrix metalloproteinase 2 (MMP-2) was purchased from Atagenix Laboratories (Wuhan, China). SCC-15 cells were obtained from the American Type Culture Collection (ATCC, VA, USA). Unless otherwise noted, all other chemicals were purchased from the Chemical Reagent Company (Beijing, China).

Synthesis of PDLLA-PEG-PDLLA triblock copolymers and HA-AC

Poly(D,L-lactide)-poly(ethylene glycol)-poly(D,L-lactide) (PDLLA-PEG-PDLLA) and acrylated hyaluronic acid (HA-AC) were synthesized as previously described.[23]

Preparation of drug nanoparticles by solvent precipitation

After 20 mg of DOX·HCl dissolved in 0.5 mL of solvent DMSO, 16 μL of triethylamine (TEA) was added into the solution to neutralize the HCl of DOX·HCl for 5 min. Then, the DOX solution was rapidly injected into the anti-solvent, 10 mL of PBS (150 mM, pH = 7.4) containing 200 mg PDLLA-PEG-PDLLA, by a pipette with vigorous stirring for 1 h at room temperature. The suspension was dialyzed against deionized water using a dialysis bag with a MWCO of cut-off 3500 Da for 4 hours and repeated more than 3 times to remove unloaded DOX and DMSO. Finally, the suspension was freeze-dried to obtain DOX nanoparticles (NanoDOX) NanoDOX powder. The same method was used to prepare SUN nanoparticles (NanoSUN).

Preparation of nano drug-loaded HA hydrogel

The lyophilized nano drug powder was dispersed in triethanolamine buffer (300 mM, pH 10.0) at a certain drug concentration under ultrasonication for several minutes. HA-AC was dissolved in the solution at 80 mg mL^{-1}, and MMP-sensitive peptides were dissolved at 20 mg mL^{-1}. Nano drug-loaded HA hydrogel was formed by mixing these two kinds of solution within 5 minutes. Here, MMP-HA hydrogel is named HM, NanoDOX-loaded HM is named NDHM, NanoSUN-loaded HM is named NSHM, and NanoDOX and NanoSUN-loaded HM is named NDSHM.

Morphology and characterization of nano drugs

After ultrasonication for 5 minutes, the hydrodynamic particle size and zeta potential of the nano-drug suspensions were measured using a Zetasizer Nano ZSP (Malvern Instruments). The suspension droplets of nano drugs are deposited on silicon wafers. Upon drying, the morphology of nanodrugs was observed using TEM. The drug-loaded hydrogel disk was snapped in the middle and freeze-dried, then observed *via* SEM to examine the cross-section.

In vitro drug release from HA hydrogel

The release behaviors of these two kinds of nano-drug-loaded HA hydrogels were independently studied in PBS (150 mM, pH = 7.4). The slice (150 μL) of nano drug-loaded HA hydrogel and 0.5 mL PBS buffer with or without MMP-2 was packed into a dialysis bag (MWCO = 3500 Da), which was subsequently placed inside a sealed glass bottle containing 5 mL of fresh PBS (150 mM, pH = 7.4). The bottles were shaken at 100 rpm at 37 °C in the dark. At predetermined intervals, 2 mL of release medium was withdrawn from the bottles and replaced with 2 mL of fresh PBS (150 mM, pH = 7.4). The release drug concentrations of the release mediums were measured at 488 nm.

In vitro cellular uptake

SCC-15 cells were seeded at a density of 8 × 104 cells per well in an 8-well LabTek chambered over glass system. After growing overnight, cells were incubated with normal saline (NS), free DOX, NanoDOX, or NDHM for 12 h. The cellular uptake of DOX

was investigated by using confocal laser scanning microscopy (CLSM, TCSSP2, Leica, Germany).

In vitro live-dead assay

SCC-15 cells were seeded at a density of 8 × 104 cells per well in 8-well Tab Tek Chambered Cover glass systems. After being allowed to grow overnight, cells were incubated with normal saline (NS), free DOX, NanoDOX, or NDHM for 24 h. A live/dead viability/cytotoxicity kit (Molecular Probes, Eugene, OR) was used to stain the cells, followed by imaging with a CLSM.

In vitro apoptosis assay

SCC-15 cells were seeded at a density of 8 × 104 cells per well in 8-well Tab Tek Chambered Cover glass systems. After being allowed to grow overnight, cells were incubated with normal saline (NS), free DOX, NanoDOX, or NDHM for 24 h. Cells were stained by annexin V-FITC and PI and imaged with a CLSM.

Animal model

BALB/c nude mice (female, 4 ∼ 6 weeks old, 16 ∼ 18 g body weight) were purchased from Vital River Laboratory Animal Technology Co. Ltd. (Beijing, China). All animal procedures were performed following the Guidance Suggestions for the Care and Use of Laboratory Animals and approved by the Institutional Animal Care and Use Committee of Beijing Vital River Laboratory Animal Technology Co. Ltd.

A nude mice model of local cancer recurrence *in vivo* was established as described by Qi.[24] Briefly, SCC-15 cells (5×10^6 cells per mouse) were subcutaneously injected into the right upper back of the mouse. When tumors reached around 200 mm^3, they were resected, and little original tumor mass was left to mimic the inevitable halfway resection on the surgical therapy. The tumors' presence was monitored, and the volume of any tumors detected was calculated using the formula:

$$\text{Tumor volume} = \frac{\text{tumor lenght} \times \text{tumor width}^2}{2} \times 100\%$$

Mice were euthanized when they exhibited signs of impaired health or when the volume of the tumor exceeded 2000 mm^3.

In vivo fluorescence imaging

After the nude mice model of local cancer recurrence *in vivo* was established, mice were randomized into three treatment groups and treated locally with NS, free DOX (the dose of DOX at 5 mg kg^{-1}), and NDHM (the dose of DOX at 5 mg kg^{-1}), respectively. The distributions of DOX were imaged using IVIS after 0 h, 2 h, 6 h, 12 h, 24 h, 72 h and 168 h.

Cancer recurrence prevention

The nude mice with tumor resection were randomly divided into three groups (5 mice per group). After being treated with NS, free DOX (DOX·HCl, the dose of DOX at 5 mg kg^{-1}), and NDHM (the dose of DOX at 2.5 mg kg^{-1}), the mice were monitored for local cancer recurrence that was defined as tumor(s) present anywhere on the back of animals under investigation. The tumor volumes and the general condition of the mice were recorded twice weekly. When the tumor volume exceeded 1000 mm^3, the mice were euthanized. The survival of the mice was monitored. Some mice after treatment were euthanized after 18 d, and their organs (brain, heart, liver, spleen, lungs, and kidneys) and tumors were harvested and fixed in para-formaldehyde. The histopathological changes in the tumor tissue were confirmed by staining with hematoxylin–eosin (H&E) terminal deoxynucleotidyl transferase-mediated dUTP nick end labeling (TUNEL) or CD31. To systematically study the effects of NDHM on the whole body of nude mice, the main excised organs were stained with H&E.

Statistical analysis

All statistical analyses were performed using GraphPad (InStat, CA, USA). All error bars used in this report are mean ± SD or SEM of at least three independent experiments. Statistically significant *p*-values are less than 0.05 ($^*P < 0.05$, $^{**}P < 0.01$, and $^{***}P < 0.001$).

Results

Morphology and characterization of nano drug and drug-loaded hydrogel

In our previous work, we used HA hydrogel as a sustained-release carrier to load DOX and SUN separately and achieved antitumor therapeutic effects in mouse models.[23,25] In this study, we further explored the combined effects of these two drugs. First, we prepared DOX and SUN nanoparticles using PDLLA-PEG-PDLLA. The encapsulation efficiencies of NanoDOX and NanoSUN are 70.1% and 86.5% respectively. The mean sizes of NanoDOX and NanoSUN were about 200 nm and 50 nm, while their zeta potentials were −7.54 mV and −6.69 mV,

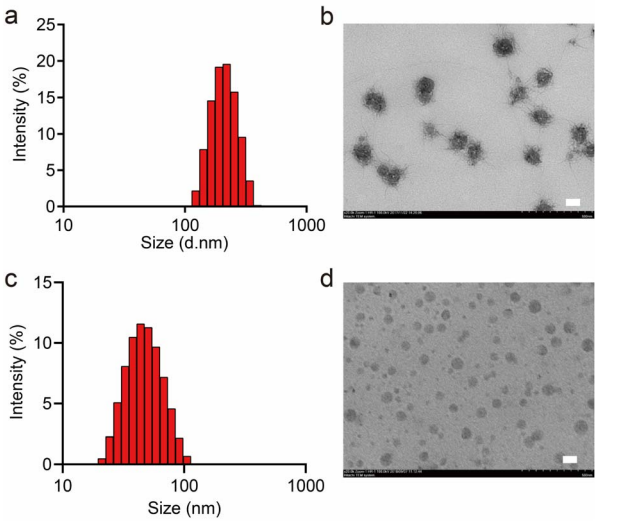

Fig. 1 The characterization of nano drug. The size (a) and TEM image (b) of DOX. The size (c) and TEM image (d) of sunitinib. The scale bars are 100 nm.

respectively (Fig. 1a and c). The microstructure of nanoparticles was further observed by TEM. NanoDOX is like cotton thread balls with a dark center, and nanoSUN is relatively regular (Fig. 1b and d). The microstructure of the hydrogel was observed by SEM. Many cavities were found inside the hydrogel, and the nanometer spherical structure was observed on the wall of the cavity (Fig. 2a and c).

Release behavior of drugs from the hydrogel

Then, NanoDOX and NanoSUN were loaded into HA hydrogels, respectively. The drug-loaded hydrogels were incubated in the presence and absence of MMP-2 in a neutral buffer to study the release behavior of drugs from the hydrogel. As expected, the drugs were slowly released from the hydrogels. The cumulative dissolution of DOX after 24 days of incubation in the presence of MMP-2 exceeds 50%, compared with less than 35% in the absence of MMP-2. Similarly, the cumulative dissolution of SUN after 14 days of incubation in the presence of MMP-2 reached up to 98%, compared to less than 80% in the absence of MMP-2. The MMP-responsive release behaviors were attributed to the increasing degradation of HA hydrogels in a buffer containing MMP-2. It is demonstrated that HA hydrogels have an outstanding long-term sustained drug release property (Fig. 2b and d).

Cellular uptake of drug in hydrogel

Relying on the unique fluorescence characteristics of DOX, the cellular uptake of DOX in the hydrogel was studied. In Fig. 3, we found that compared with the free DOX group, the cellular uptake ability is relatively higher in the NanoDOX group, indicating that the biocompatible shell of NanoDOX can better deliver it to cells and better avoid drug resistance of tumor cells. The cell uptake ability of the NDHM group was lower than the NanoDOX group but also much higher than the free DOX group, suggesting the slow-release effect of hydrogels on drugs.

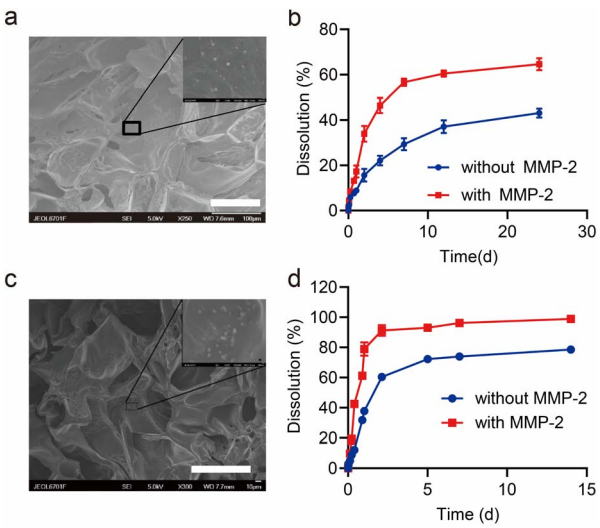

Fig. 2 The characterization of drug-loaded hydrogels. The nanostructure (a) and drug release (b) of DOX-loaded hydrogel. And the nanostructure (c) and drug release (d) of the sunitinib-loaded hydrogel.

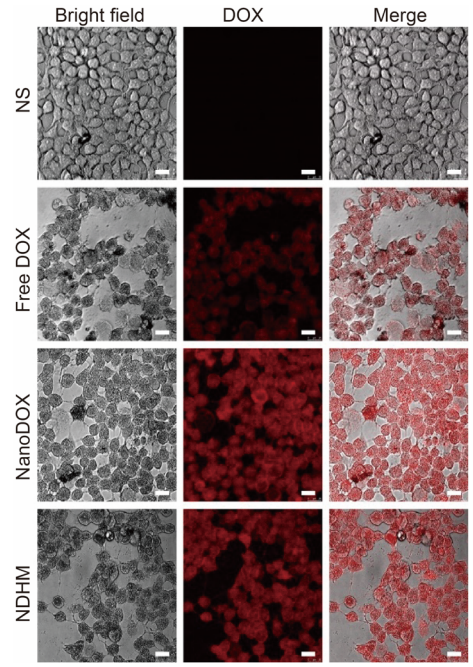

Fig. 3 The cellular uptake of drug in hydrogel. The scale bar is 10 μm.

NDSHM inhibits the activity of cells and induces apoptosis

To investigate the antitumor efficiency of NDSHM *in vitro*, a live/dead viability kit assay was performed 24 hours after exposure to various experimental groups. NS or blank hydrogel groups did not inhibit the viability of SCC-15 cells after 24 h, suggesting good biological safety of hydrogel. While in free DOX and NDHM groups, the dead cells were observed and stained red, indicating the anti-tumor efficiency of DOX. In NDSHM groups, more dead cells were detected by the kit, suggesting the best antitumor efficiency (Fig. 4a). Considering the antiangiogenic ability of sunitinib, the effect of NDSHM on human umbilical vein endothelial cells (HUVEC) was also evaluated, and we reached a similar conclusion (Fig. 5a).

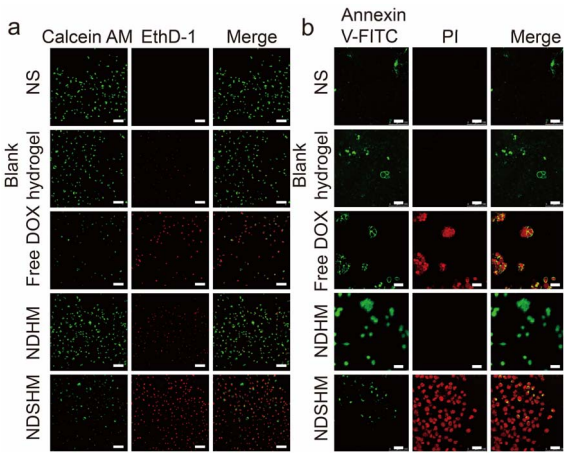

Fig. 4 The live/dead measurement (a) and apoptosis detection (b) of drug-loaded hydrogels on SCC-15 cells. The scale bar is 100 μm in (a), and the scale bar is 50 μm in (b).

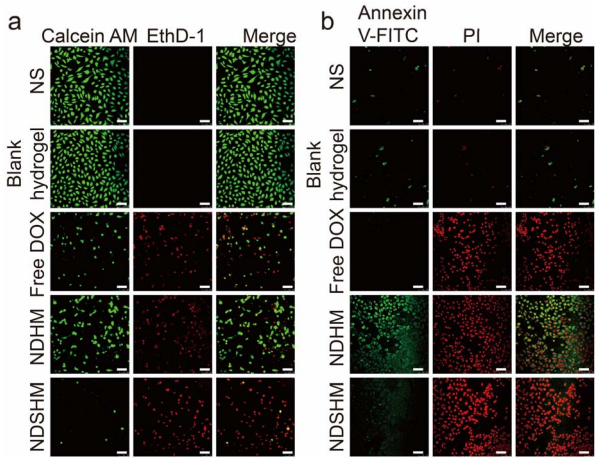

Fig. 5 The live/dead measurement (a) and apoptosis detection (b) of drug-loaded hydrogels on HUVEC cells. The scale bar is 100 μm.

Quantitative statistical analysis of live/dead cells showed that for SCC-15 cells, free DOX killed 81% of cells, NDHM killed 51% of cells, and NDSHM killed 94% of cells. For HUVECs, free DOX killed 52% of cells, NDHM killed 19% of cells, and NDSHM killed 95% of cells. These results indicate that hydrogels loaded with two drugs exhibit stronger inhibitory effects on tumor cells and vascular endothelial cells *in vitro* than hydrogels loaded with a single drug. To further clarify the specific form of cell death, an apoptosis assay was performed as a priority. We found many FITC-positive and PI-negative cells can be detected with the treatment of NDSHM, and the number was much more than that of other groups (Fig. 4b and 5b). All the results above showed that NDSHM inhibits cell viability *in vitro*, and apoptosis is the main form of cell death.

In vivo biodistribution and imaging of NDSHM

The biodistribution of NDHM was assessed using an *in vivo* imaging system. As shown in Fig. 6a, free DOX and NDHM were injected into the tumor resection site. Approximately 6 hours after injection, the DOX fluorescence signal in the free DOX group rapidly decreased and had nearly disappeared by 72 hours. In contrast, the NDHM group exhibited a more sustained DOX fluorescence signal, with detectable fluorescence at the injection site, even on day 7.

NDSHM effectively inhibits tumor recurrence

A subcutaneous tumor recurrence model was established to evaluate the efficacy of NDSHM. As shown in Fig. 6b, mice in the NS group exhibited nearly complete local tumor recurrence. In contrast, the NDHM group reduced the recurrence rate within 20 days compared to the control group. Notably, NDSHM significantly decreased local tumor recurrence compared with NDHM. Additionally, NDSHM treatment significantly extended the median survival time (Fig. 6c). To further assess whether NDSHM promotes tumor tissue apoptosis *in vivo*, TUNEL immunofluorescence staining was performed on tumor sections. As shown in Fig. 6d, NDSHM induced more apoptotic

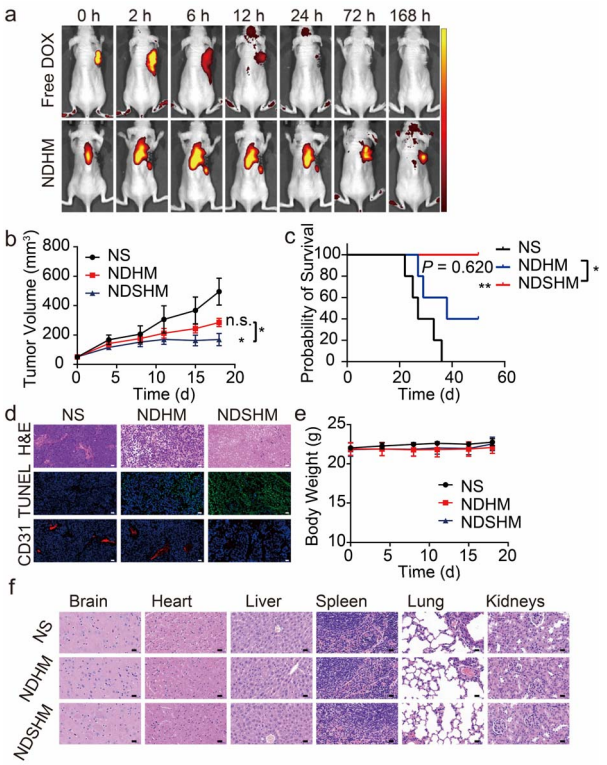

Fig. 6 *In vivo* experiments for hydrogels. (a) The *in vivo* distribution of nude mice model of local cancer recurrence treated for free DOX or NDHM (the dose of DOX at 2.5 mg kg^{-1}). The tumor growth (b) and the survival (c) of nude mice model of local cancer recurrence treated with NS, NDHM or NDSHM. (d) The H&E, TUNEL, and CD31 staining for the tumors from different groups. Blue represents the nucleus, green represents apoptotic cells, and red represents CD31-positive cells. The scale bar is 100 μm. (e) The mice weight change of different groups. (f) The H&E staining for the main organs from different groups. The scale bar is 100 μm.

cells in tumor tissue than the control and NDHM groups. Furthermore, CD31 staining, a marker of tumor angiogenesis, revealed no significant inhibition of angiogenesis in the NDHM-treated tumors. As expected, NDSHM inhibited tumor angiogenesis (Fig. 6d). Notably, there were no significant changes in body weight across any treatment groups (Fig. 6e), and neither NDSHM nor NDHM therapy induced significant toxicity (Fig. 6f). These results suggest that co-delivery of DOX and SUN using MMP-responsive hydrogel offers a promising approach to prevent OSCC recurrence.

Conclusions

This study expanded upon our previous work by utilizing the MMP-responsive hydrogel to encapsulate nano-sized doxorubicin (DOX) and nano-sunitinib. This dual-drug delivery system aims to prevent postoperative recurrence of OSCC through a combination of chemotherapy and targeted therapy.

OSCC poses a significant threat to human health. Despite continuous treatment concept and method advancements over the past 30 years, the overall therapeutic outcomes remain

limited. The 5 year survival rate for OSCC patients remains around 60%, and for those with advanced-stage disease, it is less than 30%. Postoperative recurrence is a major cause of mortality in OSCC patients, often resulting from incomplete surgical resection. While surgery remains the cornerstone of treatment, it presents considerable challenges due to the complex anatomy and essential functional structures within the oral cavity. Furthermore, there is ongoing debate regarding the definition of safe surgical margins. The controversy centers on whether the margin should be determined by the distance between the surgical cut and the leading edge of tumor invasion or by the degree of epithelial dysplasia at the margin. This uncertainty complicates the assessment of surgical outcomes, the guidance of postoperative adjuvant treatments, and the prediction of patient prognosis. If residual tumor cells remain at the surgical site, the risk of local recurrence, invasion, and metastasis increases, ultimately reducing patient survival rates.

Given the above clinical bottlenecks, our drug loading system can directly play a targeted role: (1) the biocompatibility and stable degradation ability of hydrogels can ensure that they will not cause rejection when placed in the operation area; (2) matrix metalloproteinase responsive hydrogels can sense the trend of tumor cell pre-invasion and metastasis earlier, and then accelerate the degradation of hydrogels and drug release; (3) the broad-spectrum anticancer drug DOX can significantly inhibit the malignant proliferation of residual tumor cells, thereby preventing local recurrence; (4) sunitinib, a multipoint inhibitor, can specifically block the anti-angiogenesis related signal pathways, such as VEGF/PDGF/KIT, thus preventing tumor metastasis and recurrence. The combination of advantages finally led to the realization of a new strategy of cooperative treatment for preventing postoperative recurrence of OSCC.

There are still some limits to this work. In the previous study, sunitinib nanoparticles can still play their role in anti-tumor angiogenesis through local administration. However, sunitinib does not have fluorescence properties compared with DOX, so it is difficult to evaluate its ability to cell uptake *in vitro* and metabolism distribution *in vivo* through fluorescence monitoring. Therefore, in the following study, we will try to connect the fluorescent label to sunitinib nanoparticles to realize real-time tracking. In addition, for advanced OSCC, local drug delivery carriers have certain limitations because they cannot better control tumor cells that colonize the whole body, such as circulating tumor cells (CTCs), so more drug delivery systems that can be administered throughout the body must be developed.

In conclusion, as one of the series of our studies on the application of enzyme-responsive hydrogel used in the anti-tumor field, this work provides a chemo-molecular targeted synergistic treatment strategy for preventing postoperative recurrence of OSCC.

Data availability

Data for this article, including PPT, are available at Harvard Dataverse: **https://doi.org/10.7910/DVN/5JYCT6**.

Author contributions

W. L., J. Z., and Z. F. conceived the idea, analyzed the data, and wrote the manuscript. Y. W., H. M., M. Y., C. L., and Y. W. performed experiments. All authors contributed to the discussion and editing of the manuscript.

Conflicts of interest

There are no conflicts to declare.

Acknowledgements

This work was supported by the Wu Jieping Medical Foundation Special Research Fund (grant no. 320.6750.2023-05-59).

References

1 A. C. Chi, T. A. Day and B. W. Neville, *Ca-Cancer J. Clin.*, 2015, **65**, 401–421.
2 S. A. Gharat, M. M. Momin and C. Bhavsar, *Crit. Rev. Ther. Drug Carrier Syst.*, 2016, **33**, 363–400.
3 S. Yanamoto, M. Otsuru, Y. Ota, M. Okura, T. Aikawa, H. Kurita, T. Kamata, T. Kirita, N. Yamakawa, M. Ueda, T. Yamashita, T. Komori, T. Shigeta, S. Yokoo, M. Ogawa, M. Umeda and Japan Oral Oncology Group, *Ann. Surg. Oncol.*, 2015, **22**, 992–999.
4 T. Mücke, M. Konen, S. Wagenpfeil, M. R. Kesting, K.-D. Wolff and F. Hölzle, *Ann. Surg. Oncol.*, 2011, **18**, 2739–2747.
5 I. Mohamad, M. D. E. Glaun, K. Prabhash, A. Busheri, S. Y. Lai, V. Noronha and A. Hosni, *American Society of Clinical Oncology Educational Book*, 2023, p. e389810, DOI: **10.1200/edbk_389810**.
6 Y. Tan, Z. Wang, M. Xu, B. Li, Z. Huang, S. Qin, E. C. Nice, J. Tang and C. Huang, *Int. J. Oral Sci.*, 2023, **15**, 44.
7 M. Brandwein-Gensler, M. S. Teixeira, C. M. Lewis, B. Lee, L. M. Rolnitzky, J. J. Hille, E. M. Genden, M. L. Urken and B. Y. Wang, *Am. J. Surg. Pathol.*, 2005, **29**, 167–178.
8 M. D. Kernohan, J. R. Clark, K. Gao, A. Ebrahimi and C. G. Milross, *Arch. Otolaryngol. Head Neck Surg.*, 2010, **136**, 1235–1239.
9 T.-Y. Huang, L.-P. Hsu, Y.-H. Wen, T.-T. Huang, Y.-F. Chou, C.-F. Lee, M.-C. Yang, Y.-K. Chang and P.-R. Chen, *Oral Oncol.*, 2010, **46**, 49–55.
10 H. M. W. Verheul and H. M. Pinedo, *Clin. Breast Cancer*, 2000, **1**, S80–S84.
11 R. Lugano, M. Ramachandran and A. Dimberg, *Cell. Mol. Life Sci.*, 2020, **77**, 1745–1770.
12 M. W. Dewhirst and T. W. Secomb, *Nat. Rev. Cancer*, 2017, **17**, 738–750.
13 R. Roskoski, *Biochem. Biophys. Res. Commun.*, 2007, **356**, 323–328.
14 Q. Qian, J. Song, C. Chen, Q. Pu, X. Liu and H. Wang, *Biomater. Sci.*, 2023, **11**, 2678–2692.
15 W. Zhu, Z. Zhou, M. Yang, X. Chen, S. Zhu, M. Yu, Z. Yu, W. Wu and H. Liu, *Small*, **20**, 2309476.

16 C. Cai, W. Wang, J. Liang, Y. Li, M. Lu, W. Cui, C. Fan, L. Deng, Y. Li, F. Wang and S. Liu, *Adv. Funct. Mater.*, 2021, **31**, 2008364.
17 J. Yan, Z. Zhang, X. Zhan, K. Chen, Y. Pu, Y. Liang and B. He, *Nanoscale*, 2021, **13**, 9577–9589.
18 M. Shahriari, M. Zahiri, K. Abnous, S. M. Taghdisi, M. Ramezani and M. Alibolandi, *J. Controlled Release*, 2019, **308**, 172–189.
19 Z. Zhao, J. Shen, L. Zhang, L. Wang, H. Xu, Y. Han, J. Jia, Y. Lu, R. Yu and H. Liu, *Biomater. Sci.*, 2020, **8**, 5306–5316.
20 E. Larrañeta, S. Stewart, M. Ervine, R. Al-Kasasbeh and R. F. Donnelly, *J. Funct. Biomater.*, 2018, **9**, 13.
21 G. S. Papaetis and K. N. Syrigos, *BioDrugs*, 2009, **23**, 377–389.
22 U.-J. Yun, J.-H. Lee, J. Shim, K. Yoon, S.-H. Goh, E. H. Yi, S.-K. Ye, J.-S. Lee, H. Lee, J. Park, I. H. Lee and Y.-N. Kim, *Lab. Invest.*, 2019, **99**, 1157–1172.
23 W. Li, C. Tao, J. Wang, Y. Le and J. Zhang, *RSC Adv.*, 2019, **9**, 31264–31273.
24 Y. Qi, H. Min, A. Mujeeb, Y. Zhang, X. Han, X. Zhao, G. J. Anderson, Y. Zhao and G. Nie, *ACS Appl. Mater. Interfaces*, 2018, **10**, 6972–6981.
25 Z. Fu, H. Li, P. Xue, H. Yu, S. Yang, C. Tao, W. Li, Y. Wang, J. Zhang and Y. Wang, *Front. Bioeng. Biotechnol.*, 2022, **10**, 881544.